Finite size scaling in CP^{N-1} models

Paolo Rossi and Ettore Vicari
Dipartimento di Fisica dell'Università and Istituto Nazionale di Fisica Nucleare, I-56126 Pisa, Italy
(Received 15 December 1992)

Finite size effects in Euclidean CP^{N-1} models with periodic boundary conditions are investigated by means of the $1/N$ expansion and by Monte Carlo simulations. Analytic and numerical results for the magnetic susceptibility and correlation length are compared and found to agree for small volumes. For large volumes a discrepancy is found and explained as an effect of the physical bound-state extension. The leading-order finite size effects on the Abelian string tension are computed and compared with simulations finding agreement. The finite size dependence of topological quantities is also discussed.

PACS number(s): 11.15.Ha, 11.15.Pg, 75.10.Hk

I. INTRODUCTION

The study of the finite size effects has become an important tool in the theoretical and numerical analysis of critical systems and lattice field theories.

Finite size scaling may be used in order to improve the extrapolation of finite lattice results to the infinite volume limit relevant to field-theoretical predictions. More naively, knowledge of the volume dependence of lattice results in sufficiently large volumes allows one to choose lattices such that finite size effects may be consistently smaller than the intrinsical error of numerical simulations.

Within our program of studying analytically and numerically two-dimensional CP^{N-1} models as a prototype for lattice QCD, we decided to explore their finite-volume behavior with special emphasis on two peculiar properties that our model shares with QCD: the existence of a linear confining potential and nontrivial topological properties.

CP^{N-1} models are $1/N$ expandable: we can, therefore, for sufficiently large N, make theoretical predictions on the size and pattern of finite lattice effects. This chance, in conjunction with the opportunity of performing high-statistics Monte Carlo simulations for intermediate values of N with an acceptable computer effort, offers the possibility of a systematic study of finite size effects.

This paper is organized as follows.

In Sec. II we review the theory of finite size scaling in the context of the $1/N$ expansion.

In Sec. III we discuss the lattice formulation adopted, introduce the physical observables (magnetic susceptibility and correlation length), and evaluate the order 1 and $O(1/N)$ contributions to their finite size functions.

In Sec. IV we perform the same analysis for the leading-order contribution to the Abelian string tension.

In Sec. V we present the results of numerical Monte Carlo simulations for selected values of N, from $N = 2$ to $N = 100$, and compare them to our theoretical predictions, explaining the discrepancies, when present.

In Sec. VI we draw some (hopefully general) conclusions.

II. FINITE SIZE SCALING AND $1/N$ EXPANSION

Finite size scaling in the $1/N$ expansion has been introduced and discussed in Ref. [1]. We recall here the main results adapting them to the specific context of CP^{N-1} models. Any coordinate-independent physical quantity will in general depend on four different parameters:

$$Q = Q(g, a, L, N), \tag{1}$$

where g is the coupling, L^d is the physical volume in d dimensions, and a the lattice spacing. However in the critical region $g \to g_c$ and in the infinite-volume limit all dependences on a and g may be absorbed in the dependence on the correlation length:

$$\xi \propto a \exp\left(\int^g \frac{dg'}{\beta(g')}\right) . \tag{2}$$

The finite size scaling relation amounts to the statement that, when $\xi \to \infty$ while keeping L/ξ finite, we should get

$$\frac{Q(g, a, L, N)}{Q(g, a, \infty, N)} \longrightarrow f^{(Q)}(L/\xi, N) . \tag{3}$$

The $1/N$ expandability implies that, assuming

$$Q(g, a, L, N) = Q_0(Ng, a, L) + \frac{1}{N} Q_1(Ng, a, L) + O\left(\frac{1}{N^2}\right) \tag{4}$$

and

$$\xi(g, N) = \xi_0(Ng) + \frac{1}{N}\xi_1(Ng) + O\left(\frac{1}{N^2}\right) , \tag{5}$$

we may expand the finite size functions $f^{(Q)}$ in the form

$$f^{(Q)}(L/\xi,N) = f_0^{(Q)}(L/\xi) + \frac{1}{N} f_1^{(Q)}(L/\xi) + O\left(\frac{1}{N^2}\right) , \tag{6}$$

and obtain the representations

$$\frac{Q_0(Ng,a,L)}{Q_0(Ng,a,\infty)} \longrightarrow f_0^{(Q)}(L/\xi_0), \tag{7}$$

$$\frac{Q_1(Ng,a,L)}{Q_0(Ng,a,L)} - \frac{Q_1(Ng,a,\infty)}{Q_0(Ng,a,\infty)} + \frac{L}{\xi_0}\frac{f_0'^{(Q)}(L/\xi_0)}{f_0^{(Q)}(L/\xi_0)}\frac{\xi_1}{\xi_0} \longrightarrow \frac{f_1^{(Q)}(L/\xi_0)}{f_0^{(Q)}(L/\xi_0)} . \tag{8}$$

III. LATTICE FORMULATION

Our choice of a lattice action for CP^{N-1} models is [2]

$$S_g = -\frac{1}{g}\sum_{n,\mu}\left(\bar{z}_{n+\mu} z_n \lambda_{n,\mu} + \bar{z}_n z_{n+\mu}\bar{\lambda}_{n,\mu} - 2\right), \qquad g = \frac{1}{N\beta} , \tag{9}$$

where z_n is an N-component complex scalar field, constrained by the condition $\bar{z}_n z_n = 1$ and $\lambda_{n,\mu}$ is a U(1) gauge field satisfying $\bar{\lambda}_{n,\mu}\lambda_{n,\mu} = 1$.

Observable physical quantities must be gauge invariant; we therefore focus on the correlations of the composite operator,

$$P_{i,j}(x) = \bar{z}_i(x) z_j(x) , \tag{10}$$

and specifically on the two-point function

$$G_P(x) = \langle \mathrm{Tr} P(x) P(0)\rangle_c . \tag{11}$$

Starting from the continuum definition of magnetic susceptibility,

$$\chi_m = \int d^2x\, G_P(x), \tag{12}$$

and the ($1/N$ expandable) correlation length [3]

$$\xi^2 = \frac{\int d^2x\, \frac{1}{4}x^2 G_P(x)}{\int d^2x\, G_P(x)} , \tag{13}$$

we can introduce their counterparts on finite lattices with periodic boundary conditions. Let us first define the finite lattice Fourier transform of the correlation function:

$$\widetilde{G}_P(k;L) = \frac{1}{L^2}\sum_{m,n}\langle \mathrm{Tr} P(m) P(n)\rangle_c \exp\left[\frac{2i\pi}{L}(m-n)\cdot k\right] \tag{14}$$

defined on integer values of the components of k. We then define

$$\chi_m(L) = \widetilde{G}_P(0,0;L) \underset{L\to\infty}{\longrightarrow} \chi_m , \tag{15}$$

$$\xi^2(L) = \frac{1}{4\sin^2 \pi/L}\left[\frac{\widetilde{G}_P(0,0;L)}{\widetilde{G}_P(1,0;L)} - 1\right] \underset{L\to\infty}{\longrightarrow} \xi^2 . \tag{16}$$

Within the $1/N$ expansion the following relationship holds [3]:

$$\widetilde{G}_P(k;L) = \beta^{-2}\left[\Delta_{(\alpha)}^{-1}(k;L) + \frac{1}{N}\Delta_1^{-1}(k;L) + O\left(\frac{1}{N^2}\right)\right] , \tag{17}$$

where, in the infinite lattice notation,

$$\Delta_{(\alpha)}^{-1}(k) = \int \frac{d^2q}{(2\pi)^2}\frac{1}{[\widehat{q}^2 + m_0^2]\left[\widehat{(k+q)}^2 + m_0^2\right]} , \tag{18}$$

$$\Delta_1^{-1}(k) = -\int \frac{d^2q}{(2\pi)^2}\Delta_{(\alpha)}(q) V_{(\alpha)}(q,k) + \int \frac{d^2q}{(2\pi)^2}\Delta_{(\lambda)}(q) V_{(\lambda)}(q,k) + \frac{1}{2}\Delta_{(\alpha)}(0)\frac{\partial}{\partial m_0^2}\Delta_{(\alpha)}^{-1}(k)\int \frac{d^2q}{(2\pi)^2}\left[\Delta_{(\alpha)}(q)\frac{\partial}{\partial m_0^2}\Delta_{(\alpha)}^{-1}(q) + \Delta_{(\lambda)}(q)\frac{\partial}{\partial m_0^2}\Delta_{(\lambda)}^{-1}(q)\right] . \tag{19}$$

The auxiliary quantities we have introduced are the effective vertices

$$\Delta_{(\lambda)}^{-1}(k) = \int \frac{d^2q}{(2\pi)^2}\frac{2\sum_\mu \cos q_\mu}{\widehat{q}^2 + m_0^2} - \int \frac{d^2q}{(2\pi)^2}\frac{4\sum_\mu \sin^2(q_\mu + k_\mu/2)}{[\widehat{q}^2 + m_0^2]\left[\widehat{(q+k)}^2 + m_0^2\right]} , \tag{20}$$

$$V_{(\alpha)}(k,p) = \int \frac{d^2q}{(2\pi)^2} \frac{1}{[\hat{q}+m_0^2]^2 \left[\widehat{(q+p)}^2 + m_0^2\right] \left[\widehat{(q+k)}^2 + m_0^2\right]} + p \to -p$$
$$+ \int \frac{d^2q}{(2\pi)^2} \frac{1}{[\hat{q}+m_0^2] \left[\widehat{(q+p)}^2 + m_0^2\right] \left[\widehat{(q+k)}^2 + m_0^2\right] \left[\widehat{(q+p+k)}^2 + m_0^2\right]} , \tag{21}$$

$$V_{(\lambda)}(k,p) = \int \frac{d^2q}{(2\pi)^2} \frac{4\sum_\mu \sin^2(q_\mu + p_\mu/2)}{[\hat{q}+m_0^2]^2 \left[\widehat{(q+p)}^2 + m_0^2\right] \left[\widehat{(q+k)}^2 + m_0^2\right]} + p \to -p$$
$$+ \int \frac{d^2q}{(2\pi)^2} \frac{4\sum_\mu \sin(q_\mu + p_\mu/2)\sin(q_\mu + k_\mu + p_\mu/2)}{[\hat{q}+m_0^2] \left[\widehat{(q+p)}^2 + m_0^2\right] \left[\widehat{(q+k)}^2 + m_0^2\right] \left[\widehat{(q+p+k)}^2 + m_0^2\right]}$$
$$- \int \frac{d^2q}{(2\pi)^2} \frac{2\sum_\mu \cos q_\mu}{[\hat{q}+m_0^2]^2 \left[\widehat{(q+k)}^2 + m_0^2\right]^2} . \tag{22}$$

The conversion to a finite lattice is obtained by the replacements

$$\int \frac{d^2q}{(2\pi)^2} \longrightarrow \frac{1}{L^2} \sum_{q_\mu=1}^{L} , \tag{23}$$

and on periodic (toroidal) lattices the zero modes of the inverse propagator $\Delta^{-1}_{(\lambda)}(k)$, if nonvanishing, must be explicitly removed. Moreover

$$m_0^2 \longrightarrow m_L^2 , \tag{24}$$

where in order to keep Ng fixed we must relate m_L to m_0 by the lattice gap equation

$$\frac{1}{L^2} \sum_{q_\mu=1}^{L} \frac{1}{\hat{q}^2 + m_L^2} = \frac{1}{Ng} = \int \frac{d^2q}{(2\pi)^2} \frac{1}{\hat{q}^2 + m_0^2} = \frac{1}{2\pi} \frac{1}{1+m_0^2/4} K\left(\frac{1}{1+m_0^2/4}\right) . \tag{25}$$

This equation has been analyzed in detail in Ref. [1] for $m_0 \to 0$, i.e., in the scaling region, where

$$\int \frac{d^2q}{(2\pi)^2} \frac{1}{\hat{q}^2 + m_0^2} \underset{m_0 \to 0}{\sim} \frac{1}{4\pi} \ln \frac{32}{m_0^2} . \tag{26}$$

In the scaling region one could establish the relationship

$$z_0 \equiv m_0 L = z_c \exp\left(-\frac{\omega(z_L)}{2}\right) , \tag{27}$$

where $z_L = m_L L$, $z_c = 4.163\,948...$, and in the region $z_L \leq 2\pi$ the function ω may be defined by

$$\omega(z_L) = \frac{4\pi}{z_L^2} + 4\pi \sum_{n=1}^{\infty} (-1)^n z_L^{2n} d_{n+1} ,$$
$$d_n = \frac{1}{(2\pi)^{2n}} \sum_{m_1,m_2=-\infty}^{\infty} \frac{1}{(m_1^2+m_2^2)^n} , \quad n > 1 . \tag{28}$$

In the definition of d_n the sum must be performed excluding the term $(m_1, m_2) = (0,0)$. The function $z_0(z_L)$ is monotonic and invertible. We could therefore make use of the auxiliary variable z_L in the computations and replace it by z_0 only at the end.

In practice, in order to take into account at least some of the scaling violation effects due to irrelevant operators, we found it always convenient to solve explicitly and numerically Eq. (25) on each finite $L \times L$ lattice for an assigned value of Ng.

Let us derive the large-N results:

$$\beta^2 \chi_{m,0}(L) = \Delta^{-1}_{(\alpha)}(0,0;L) = \frac{1}{L^2} \sum_{q_\mu=1}^{L} \frac{1}{(\hat{q}^2 + m_L^2)^2}$$
$$= -\frac{\partial \beta}{\partial m_L^2} , \tag{29}$$

$$\beta^2 \chi_{m,0} = \int \frac{d^2q}{(2\pi)^2} \frac{1}{(\hat{q}^2 + m_0^2)^2} \underset{m_0 \to 0}{\sim} \frac{1}{4\pi m_0^2} ,$$

and

$$\xi_0^2(L) = \frac{1}{4\sin^2 \pi/L}\left[\frac{\Delta_{(\alpha)}^{-1}(0,0;L)}{\Delta_{(\alpha)}^{-1}(1,0;L)} - 1\right] \quad ,$$

$$\xi_0^2 = \lim_{L\to\infty} \xi_0^2(L) \underset{m_0\to 0}{\sim} \frac{1}{6m_0^2} \quad . \tag{30}$$

The corresponding large-N finite size functions are obtained by the relations

$$\frac{\chi_{m,0}(\beta,L)}{\chi_{m,0}(\beta,\infty)} \to f_0^{(\chi)}(L/\xi_0) \quad ,$$

$$\frac{\xi_0(\beta,L)}{\xi_0(\beta,\infty)} \to f_0^{(\xi)}(L/\xi_0) \quad , \tag{31}$$

for $\xi_0 \to \infty$ while keeping L/ξ_0 constant.

The infinite volume limit quantities can be obtained numerically by performing the calculation on very large lattices and checking the convergence of the results. For large enough lattices an extrapolation based on the formula

$$Q(L) \longrightarrow Q(\infty) + \frac{c}{L^2} \quad \text{for } L \gg 1 \quad , \tag{32}$$

gives safe results even if it does not keep into account the existing logarithmic corrections to the L^{-2} term. Furthermore, we must in principle worry about the effects due to irrelevant operators that may spoil the universal behavior by introducing a separate dependence on ξ_0^{-2}. Working at very large values of ξ_0 takes this problem partially into account. Further improvement may be obtained by considering different values of ξ_0 and linearly extrapolating in ξ_0^{-2}. For ξ_0 large enough, this extrapolation, albeit purely phenomenological because all existing logarithmic dependence on ξ_0 is not included, is powerful enough to predict results that are stable under iteration of the procedure (within the numerical precision required).

An accurate evaluation of the functions $f_0^{(\chi)}$ and $f_0^{(\xi)}$ is presented in Figs. 1 and 2, respectively. The behaviors are quite similar and are characterized by the existence of two different regimes, corresponding to different physical situations. As long as L/ξ_0 is small ($L < 5\xi_0$ say), we are exploring the small volume behavior of the system. Because of asymptotic freedom, this is an essentially perturbative, small coupling regime, and actually the finite size functions might be quite accurately evaluated within standard finite volume perturbation theory [4–6], with the only limitation of ignoring the absolute scale of the abscissa, since perturbation theory does not allow for the computation of the ratio between the mass gap and the Λ parameter which relates the quantity ΛL appearing in perturbation theory to the finite size variable L/ξ_0. When L/ξ_0 becomes large ($L > 10\xi_0$ say) we start to explore large-distance effects, that are dominated by the physical mass poles. Because of the two-particle nature

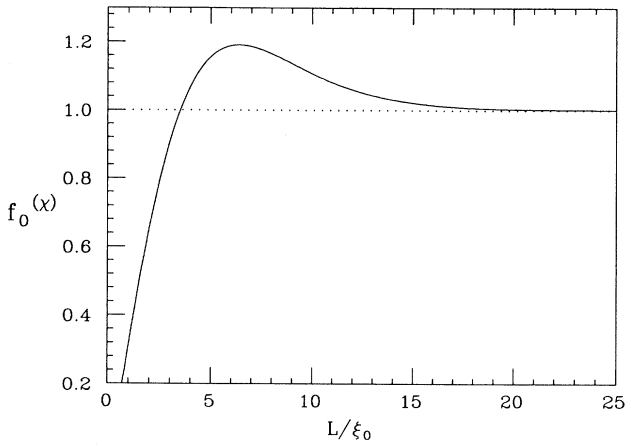

FIG. 1. Large-N finite size scaling function of the magnetic susceptibility.

of the operator (10), the functional dependence is characterized by a decrease with growing L/ξ_0 (two particles in a box effect) in contrast with the asymptotic growth characteristic of the corresponding single-particle operators (free particle in a box effect).

In the scaling region we can write $f_0^{(\chi)}$ in terms of $\omega(z_L)$; indeed we have

$$f_0^{(\chi)}(L/\xi_0) \underset{m_0\to 0}{\sim} \frac{\partial m_0^2}{\partial m_L^2} = -z_0^2 \frac{\partial \omega(z_L)}{\partial z_L^2} \quad , \tag{33}$$

which is useful for $z_L < 2\pi$. A similar formula can be obtained for $f_0^{(\xi)}$.

The determination of the $1/N$ corrections to the finite-size functions proceeds according to the general formalism [1] described in the previous section. Let us consider as an example the function $f_1^{(\chi)}$; the determination of $f_1^{(\xi)}$ involves exactly the same steps and the details will not be reported here. We may deduce from Eqs. (8), (15), and (17) the relationship

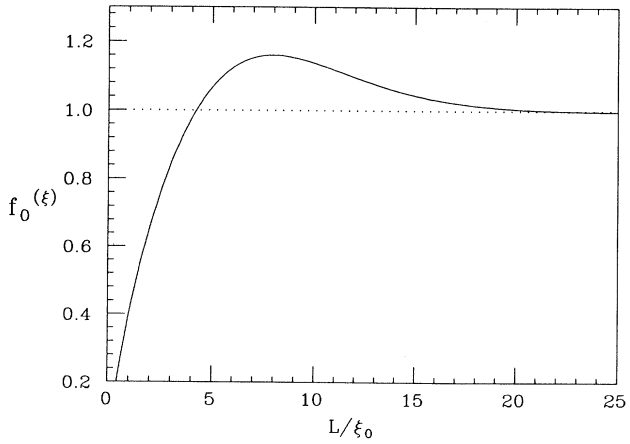

FIG. 2. Large-N finite size scaling function of the correlation length.

$$\frac{f_1^{(x)}(L/\xi_0)}{f_0^{(x)}(L/\xi_0)} = \frac{\Delta_1^{-1}(0;L)}{\Delta_{(\alpha)}^{-1}(0;L)} - \frac{\Delta_1^{-1}(0;\infty)}{\Delta_{(\alpha)}^{-1}(0,\infty)} + \frac{L}{\xi_0}\frac{f_0'^{(x)}(L/\xi_0)}{f_0^{(x)}(L/\xi_0)}\frac{\xi_1}{\xi_0} \quad , \tag{34}$$

where one can prove that

$$\Delta_1^{-1}(0) = -\frac{1}{2}\int \frac{d^2q}{(2\pi)^2}\Delta_{(\alpha)}^{-1}(0)\Delta_{(\alpha)}(q)\frac{\partial}{\partial m_0^2}\left(\Delta_{(\alpha)}(0)\frac{\partial}{\partial m_0^2}\Delta_{(\alpha)}^{-1}(q)\right) + \Delta_{(\alpha)}^{-1}(0)\Delta_{(\lambda)}(q)\frac{\partial}{\partial m_0^2}\left(\Delta_{(\alpha)}(0)\frac{\partial}{\partial m_0^2}\Delta_{(\lambda)}^{-1}(q)\right) \quad , \tag{35}$$

and its finite lattice generalization holds. The function

$$H^{(x)}(L/\xi_0) = \frac{1}{2}\frac{L}{\xi_0}\frac{f_0'^{(x)}(L/\xi_0)}{f_0^{(x)}(L/\xi_0)} = z_0^2\frac{\partial}{\partial z_0^2}\ln f_0^{(x)} \tag{36}$$

could be extracted from the definition of $f_0^{(x)}(L/\xi_0)$. In particular one can show that in the scaling region

$$H^{(x)}(L/\xi_0) \underset{m_0\to 0}{\sim} 1 - \frac{L^2}{2\pi}\frac{\sum(q^2+m_L^2)^{-3}}{\left[\sum(q^2+m_L^2)^{-2}\right]^2} = 1 - \frac{\partial^2\omega/(\partial z_L^2)^2}{\left(\partial\omega/\partial z_L^2\right)^2} \quad . \tag{37}$$

Finally we can evaluate

$$2\xi_0\xi_1 = \lim_{L\to\infty}\frac{\Delta_{(\alpha)}^{-1}(0,0;L)}{\Delta_{(\alpha)}^{-1}(1,0;L)}\frac{1}{4\sin^2\pi/L}\left[\frac{\Delta_1^{-1}(0,0;L)}{\Delta_{(\alpha)}^{-1}(0,0;L)} - \frac{\Delta_1^{-1}(1,0;L)}{\Delta_{(\alpha)}^{-1}(1,0;L)}\right] \quad . \tag{38}$$

We are now in principle ready to evaluate the $1/N$ contribution to the finite size functions of the magnetic susceptibility and of the correlation length.

There is a further subtlety one must take into account when evaluating quantities in a finite lattice. The definition of $H^{(x)}$ implies that this quantity must vanish in the $L/\xi \to \infty$ limit. Contributions from irrelevant operators may therefore become comparable to the value of the function itself in the large L regime. We must make sure that these contributions do not spoil the final result. A very simple trick amounts to replacing the definition extracted from Eq. (37) with

$$H_L^{(x)}(z_0) = 1 - \left\{\frac{\frac{1}{L^2}\sum(\hat{q}^2+m_L^2)^{-3}}{\left[\frac{1}{L^2}\sum(\hat{q}^2+m_L^2)^{-2}\right]^2}\right\}\left\{\frac{\int(\hat{q}^2+m_0^2)^{-3}}{\left[\int(\hat{q}^2+m_0^2)^{-2}\right]^2}\right\}^{-1} \quad . \tag{39}$$

Since in the scaling region

$$\frac{\int(\hat{q}^2+m_0^2)^{-3}}{\left[\int(\hat{q}^2+m_0^2)^{-2}\right]^2} \underset{m_0\to 0}{\sim} 2\pi \quad , \tag{40}$$

the two definitions differ only by irrelevant contributions. However the second definition has the property that it goes to zero when $L \to \infty$ even outside the scaling region, and therefore it will not spoil the large L behavior of the function.

The same analysis goes through in the construction of the finite size scaling function $f_1^{(\xi)}$ and we will not repeat it here. Let us only quote the final expression we adopted in the numerical calculations:

$$\begin{aligned} H_L^{(\xi)}(z_0) = z_0^2\partial\ln f_0^{(\xi)}/\partial z_0^2 &= \frac{1}{2} + \frac{1}{4\sin^2\pi/L}\frac{1}{4\pi\xi_0^2(L)}\Delta_{(\alpha)}(1,0;L) \\ &\times\left[\Delta_{(\alpha)}(1,0;L)\frac{1}{L^2}\sum\frac{1}{[\hat{q}^2+m_L^2]^2\left[\widehat{(q+l)}^2+m_L^2\right]}\right. \\ &\left.-\Delta_{(\alpha)}(0,0;L)\frac{1}{L^2}\sum\frac{1}{[\hat{q}^2+m_L^2]^3}\right] , \end{aligned} \tag{41}$$

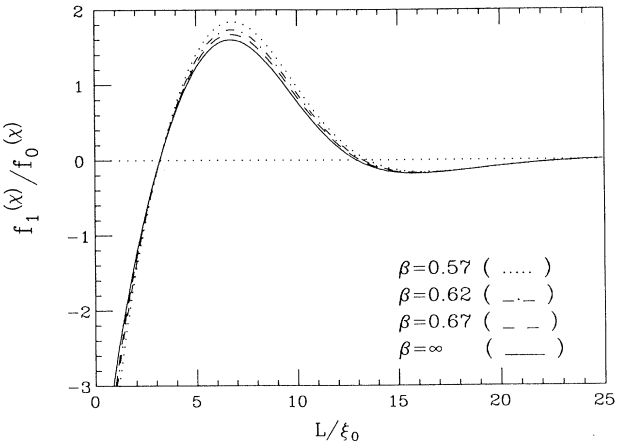

FIG. 3. $f_1^{(\chi)}/f_0^{(\chi)}$ for various values of β. The continuous line shows the $\xi \to \infty$ extrapolation.

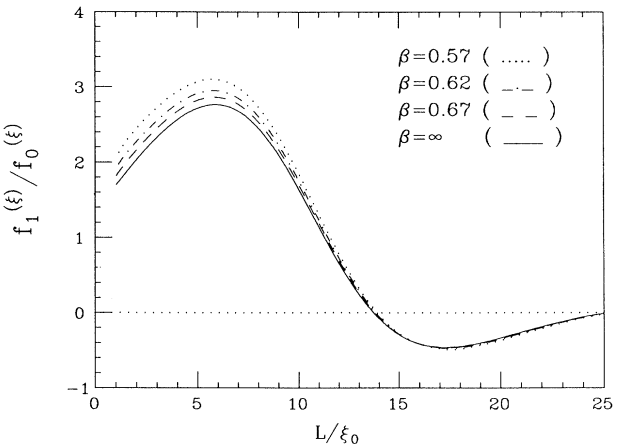

FIG. 4. $f_1^{(\xi)}/f_0^{(\xi)}$ for various values of β. The continuous line shows the $\xi \to \infty$ extrapolation.

where $l = (1,0)$.

We are now ready for a numerical evaluation of $f_1^{(\chi)}/f_0^{(\chi)}$ and $f_1^{(\xi)}/f_0^{(\xi)}$. The results are presented in Figs. 3 and 4, respectively. Values obtained at finite ξ_0, and therefore affected by the presence of nonscaling contributions, are subsequently extrapolated at infinite ξ_0, after having verified that scaling volations are well parametrized by a term proportional to ξ_0^{-2}. We estimate the error in our determinations to be uniform and to be everywhere contained within the graphical width of the line representing our results.

We notice that the behaviors are similar but they are not quite the same. In particular $f_1^{(\chi)}$ has two zeros: the smaller one lies in the perturbative region and should manifest itself in the existence of a region where the finite size function at finite N is, for N large enough, independent of N. This result will be confirmed by Monte Carlo simulations in Sec. V.

IV. STRING TENSION

Another very important physical quantity in the context of CP^{N-1} models (and of lattice gauge theories) is the string tension that may be extracted from the asymptotic area law holding for Wilson loops. Within the $1/N$ expansion, the string tension is depressed by a power of N^{-1}, and therefore it is sufficient for our purpose to focus on the first nontrivial contribution to the rectangular Wilson loop:

$$\ln W(R,T) = -\frac{1}{2N}\int \frac{d^2k}{(2\pi)^2}\frac{\sin^2\frac{k_1 R}{2}}{\sin^2\frac{k_1}{2}}\frac{\sin^2\frac{k_2 T}{2}}{\sin^2\frac{k_2}{2}}\hat{k}^2\Delta_{(\lambda)}(k) \quad . \tag{42}$$

Actually in order to extract the string tension it is convenient to study the Creutz ratios:

$$\begin{aligned}\chi_C(R,T) &= \ln\frac{W(R,T-1)\,W(R-1,T)}{W(R,T)\,W(R-1,T-1)} \\ &= \frac{1}{2N}\int \frac{d^2k}{(2\pi)^2}\frac{\sin\frac{k_1}{2}(2R-1)}{\sin\frac{k_1}{2}}\frac{\sin\frac{k_2}{2}(2T-1)}{\sin\frac{k_2}{2}}\hat{k}^2\Delta_{(\lambda)}(k) \quad ,\end{aligned} \tag{43}$$

and the Polyakov ratios

$$\chi_P(R) = \ln\frac{W(R-1,L)}{W(R,L)} = \frac{1}{2N}\int \frac{dk_1}{2\pi}\frac{\sin\frac{k_1}{2}(2R-1)}{\sin\frac{k_1}{2}}\hat{k_1}^2\Delta_{(\lambda)}(k_1,0) \quad . \tag{44}$$

In the infinite volume limit and in the scaling region, for $R,T \gg \xi_0$ one obtains

$$\begin{aligned}\chi_C(R,T) &\longrightarrow \frac{6\pi m_0^2}{N} = \frac{\pi}{N\xi_0^2} \equiv \sigma_0, \\ \chi_P(R) &\longrightarrow \sigma_0 \quad .\end{aligned} \tag{45}$$

On a finite lattice χ_C and χ_P are obtained by replacing in Eqs. (43) and (44) $\Delta_{(\lambda)}(k)$ with the finite size propagator $\Delta_{(\lambda)}(k;L)$. We may focus on the square Wilson loops ($R = T$) and compute the dimensionless quantity $C(R) = \chi_C(R,R)\xi^2$. However, when studying finite size effects, we must take into account the existence of two different physical length scales: ξ and R. Therefore, even in the scaling region we end up in a function of two variables; indeed for $\xi \to \infty$ keeping fixed the ratios L/ξ and R/ξ we must have

$$C(N,g,R,L,a) \underset{\xi\to\infty}{\sim} f^{(C)}(N,L/\xi,R/L) \underset{N\to\infty}{\sim} \frac{1}{N} f_0^{(C)}(L/\xi_0,R/L) \ . \tag{46}$$

The same relation holds for the dimensionless quantity $P(R) = \chi_P(R)\xi^2$:

$$P(N,g,R,L,a) \underset{\xi\to\infty}{\sim} f^{(P)}(N,L/\xi,R/L) \underset{N\to\infty}{\sim} \frac{1}{N} f_0^{(P)}(L/\xi_0,R/L) \ . \tag{47}$$

We evaluated the function $f_0^{(P)}$ numerically at the fixed value $\beta = 0.86$ such that $\xi_0 \approx 16$, where we checked that scaling was satisfied within 0.2%. The results are plotted in Fig. 5 for several values of L as a function of R/L. The resulting curves correspond to the sections at constant L/ξ_0 of the two-variable function $f_0^{(P)}$. This choice of variables is most adequate if we want to focus on large Wilson loops (i.e., such that $R \gg \xi$). Otherwise a more proper choice would have been the couple L/ξ_0, R/ξ_0.

Notice that even in the limit $L/\xi_0, R/\xi_0 \to \infty$ as long as the ratio R/L is nonvanishing, we do get a nontrivial function of this ratio. Since at large N, in the continuum and for infinite volume, we have that, for $k\xi_0 \to 0$,

$$\Delta_{(\lambda)}(k) \to \frac{2\pi}{\xi_0^2 k^2} \ , \tag{48}$$

we may exploit the condition $L/\xi_0 \to \infty$ with R/L finite to replace the dressed propagator $\Delta_{(\lambda)}(k;L)$ with a lattice representation of its pole part [7]:

$$\Delta_{\rm em}(k) = \frac{2\pi}{\xi_0^2 \widehat{k}^2} \ . \tag{49}$$

It is then easy to show that

$$\lim_{L/\xi_0\to\infty} f_0^{(C)}(L/\xi_0,R/L) = \pi\left[1-\left(\frac{2R-1}{L}\right)^2\right] \ , \tag{50}$$

while the corresponding computation for the Polyakov loops leads to

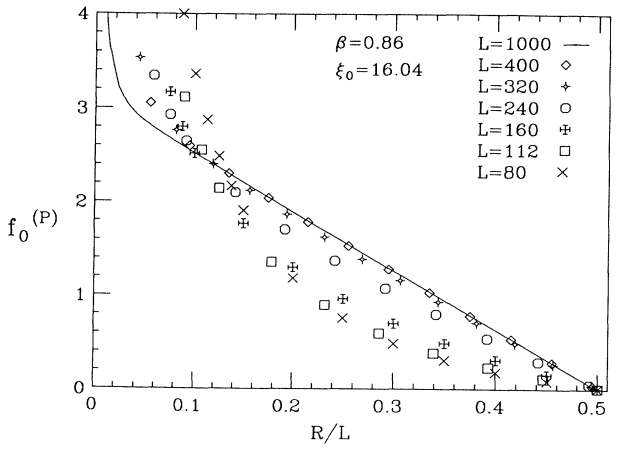

FIG. 5. $f_0^{(P)}$ versus R/L at $\beta = 0.86$.

$$\lim_{L/\xi_0\to\infty} f_0^{(P)}(L/\xi_0,R/L) = \pi\left[1-\left(\frac{2R-1}{L}\right)\right] \ . \tag{51}$$

Actually one may easily prove that the vanishing of the Creutz and Polyakov ratios at $R = (L+1)/2$ holds for any finite lattice and for any acceptable choice of the propagator $\Delta_{(\lambda)}$, and depends only on the Abelian structure of the loop variables.

We may study the lattice symmetries and further notice that

$$f_0^{(P)}(R) = -f_0^{(P)}(L+1-R) \ , \tag{52}$$

while defining the combination

$$\chi_{\rm sym}(R,T) = \chi_C(R,T) - \chi_P(R) - \chi_P(T) \ , \tag{53}$$

we find

$$\chi_{\rm sym}(R,T) = \chi_{\rm sym}(L+1-R,L+1-T) \ . \tag{54}$$

Hence

$$f_0^{\rm sym}(R) = f_0^{\rm sym}(L+1-R) \underset{L/\xi\to\infty}{\sim} -\pi\left[1-\left(\frac{2R-1}{L}\right)\right]^2 \ . \tag{55}$$

It is tempting to redefine the finite size scaling functions extracting the purely kinematical factors derived above. We shall consider for definiteness the quantity (even under the exchange $R \to L+1-R$)

$$g_0^{(P)}(L/\xi_0,R/L) = \frac{f_0^{(P)}(L/\xi_0,R/L)}{1-\left(\frac{2R-1}{L}\right)} \underset{L/\xi_0\to\infty}{\sim} \pi \ . \tag{56}$$

When $L \gg \xi_0$ we can study the regime $L > 2R \gg \xi_0$, expecting our results to be largely independent of the ratio R/ξ_0. Naively this might appear to imply that $g_0^{(P)}(L/\xi_0,R/L)$ should not depend on R/L. However this condition is realized in the following subtler way:

$$g_0^{(P)}(L/\xi_0,R/L) \to \pi + \phi(L/\xi_0)\psi(R/L) \tag{57}$$

for $L/\xi_0 \gg 1$ and $R/\xi_0 > 1$, and the function $\phi(L/\xi_0) \to 0$ for $L/\xi_0 \to \infty$.

The function $g_0^{(P)}$ has been numerically obtained directly from the above-mentioned determination of $f_0^{(P)}$ and is plotted in Fig. 6. We extracted our best determinations of the functions ϕ and ψ from an analysis of the same numerical data, when they were relevant (i.e.,

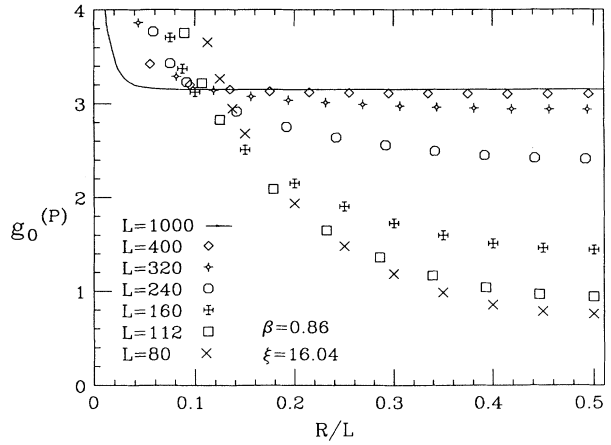

FIG. 6. $g_0^{(P)}$ versus R/L at $\beta = 0.86$.

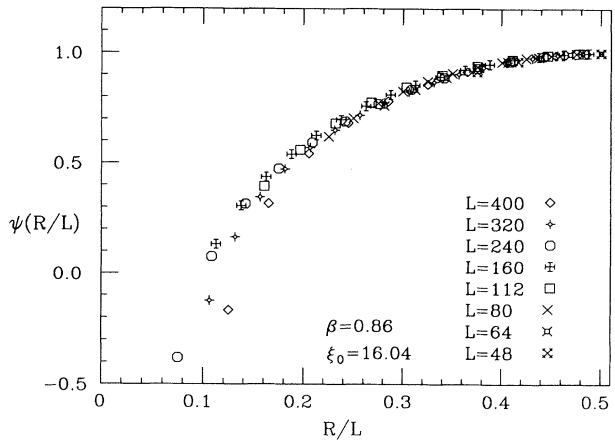

FIG. 8. $\psi(R/L)$ at $\beta = 0.86$ for several values of L.

for $R/\xi_0 > 1$). Our results are presented in Figs. 7 and 8, where we have chosen the normalization $\psi(1/2) = 1$. Studying the Creutz ratios we found a similar behavior.

The origin of the nontrivial albeit kinematical (i.e., not related to the propagation of the physical degrees of freedom) dependence in the regime $R/\xi_0 > 1$ can be traced qualitatively to the observation that, for all finite lattices, the dynamically generated massless pole in the propagator $\Delta_{(\lambda)}(k)$ does in fact disappear, and the linear confining potential is replaced, in the small k regime, by an effective Yukawa potential parametrized by a "mass" $\mu = \mu(L/\xi_0)$ becoming smaller and smaller with increasing L, and therefore approximating the linear behavior with better and better accuracy according to the relationship

$$\lim_{\mu\to 0} \frac{1 - e^{-\mu R}}{\mu} = R \quad . \tag{58}$$

The parameter $\mu(L/\xi_0)$ sets the scale of an effective long range lattice interaction; when $L/\xi_0 \to \infty$, $\mu(L/\xi_0) \to 0$, and the infinite volume physics is well approximated when $1/\mu \gg L$; but when L/ξ_0 is not too large the relationship $L > 1/\mu \gg \xi_0$ may hold. As a consequence of this phenomenon, the measured finite lattice string tension, whose operational definition might be

$$g_0^{(P)}(L/\xi_0, R/L = 1/2) \to \pi + \phi(L/\xi_0) \quad , \tag{59}$$

may turn out to be significantly different from π even for large values of L/ξ_0.

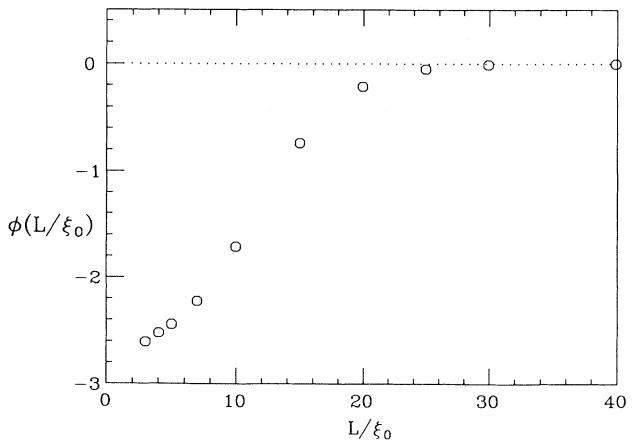

FIG. 7. $\phi(L/\xi_0)$ at $\beta = 0.86$.

In order to have a more quantitative perception of this phenomenon, we performed a study of the finite size dependence of the function $\Delta^{-1}_{(\lambda)}(k, 0; L)$, plotted in Fig. 9 as a function of the dimensionless variable $k\xi_0$ for several values of L/ξ_0. Notice that the variable $k\xi_0$ can only take discrete values, and for small L/ξ_0 these values are quite distant from each other. In Fig. 10 we plot the values of $\Delta^{-1}_{(\lambda)}(0; L) \equiv \mu^2\xi_0^2/2\pi$ against the function $(\xi_0/L)^2$ taken as an estimator of the contribution from the first nontrivial value of k. Figure 10 shows that the condition $\Delta^{-1}_{(\lambda)}(0; L) \ll (\xi_0/L)^2$ (corresponding to $L \ll 1/\mu$) holds for $L/\xi_0 \geq 25$, while for smaller L/ξ_0 significant deviations from the infinite volume behavior are to be expected, as already phenomenologically observed.

We evaluated analytically the function $g_Y^{(P)}(L/\xi_0, R/L)$ in the scaling limit, assuming an effective Yukawa propagator, and found

$$g_Y^{(P)}(L/\xi_0, R/L) = \pi \frac{\sinh\left[\frac{\mu L}{2}\left(1 - \frac{2R}{L}\right)\right]}{\sinh\left(\frac{\mu L}{2}\right)\left(1 - \frac{2R}{L}\right)} \quad , \tag{60}$$

where

$$(\mu L)^2 = 2\pi\Delta^{-1}_{(\lambda)}(0; L/\xi_0)\left(\frac{L}{\xi_0}\right)^2 \quad . \tag{61}$$

The corresponding functions

$$\phi_Y(L/\xi_0) = \pi\left[\frac{\frac{\mu L}{2}}{\sinh(\frac{\mu L}{2})} - 1\right] \tag{62}$$

and $\psi_Y(R/L)$ are plotted in Figs. 11 and 12, using the same conventions and notation of Figs. 7 and 8. The qualitative and quantitative agreement is extremely sat-

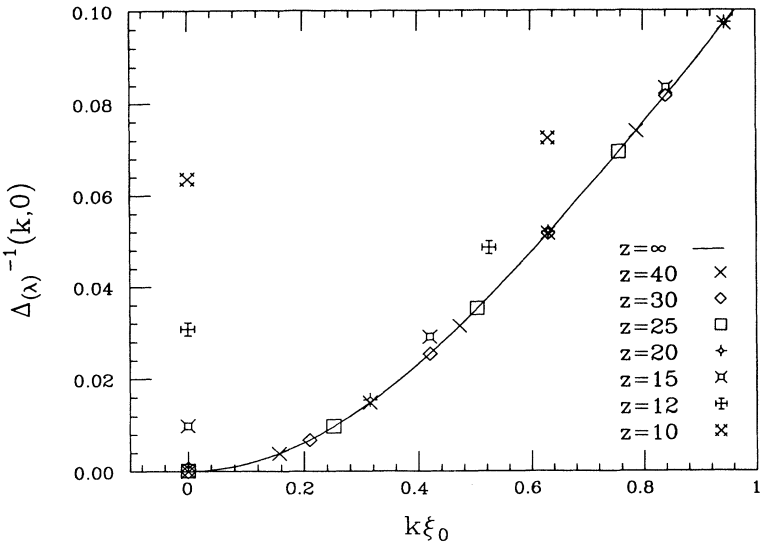

FIG. 9. $\Delta_{(\lambda)}^{-1}(k,0;L)$ versus $k\xi_0$ for several values of $z \equiv L/\xi_0$.

isfactory, in view of the crude approximations, and confirms our interpretation of this finite size effect.

Up to now we have assumed to be in the scaling region and therefore we have neglected the scaling deviations, which, at finite ξ_0, generate corrections to the value of the string tension. By using the relation

$$\frac{\chi_P(\beta,R,L)}{\left[1-\left(\frac{2R-1}{L}\right)\right]} \to \sigma_0(\beta) \tag{63}$$

for $L, R \gg \xi_0$, we extracted the value of the string tension for several values of β. The results for the dimensionless quantity $N\sigma_0\xi_0^2$ are reported in Table I and plotted in Fig. 13 versus $1/\xi_0^2$. They converge to the continuum value π, and, as expected, the scaling violations are approximately proportional to ξ_0^{-2}. From the square Creutz ratios (i.e., those with $R = T$) we obtained the same results via the relation

$$\frac{\chi_C(\beta,R,R,L)}{\left[1-\left(\frac{2R-1}{L}\right)^2\right]} \to \sigma_0(\beta) \tag{64}$$

for $L, R \gg \xi_0$.

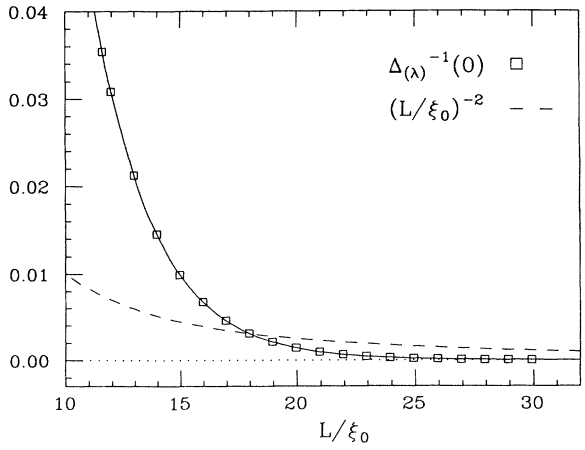

FIG. 10. $\Delta_{(\lambda)}^{-1}(0;L)$ versus L/ξ_0. The dashed line shows the function $(L/\xi_0)^{-2}$.

V. SIMULATIONS

In order to check the predictive power of the $1/N$ expansion approach to finite size scaling and to obtain results for small values of N where the expansion is not expected to give sensible information, we proceeded to Monte Carlo simulations of CP^{N-1} models for a wide spectrum of values of N. In the following we will show numerical results for $N = 2, 4, 10, 21, 41, 100$. Data for $N = 2$ and $N = 4$ were already presented in Refs. [2,7]. Summaries of the results for $N = 10, 21, 41, 100$ are given respectively in Tables II, III, IV, and V.

The action (9) is known to enjoy precocious scaling, and the chosen values of ξ are expected to be consistent with scaling violations $\sim 1\%$ for all the observables derived from the two-point function G_P [2,7,8]. In most of our simulations we employed algorithms consisting of efficient mixtures of overheated bath and microcanonical algorithms. The detailed description of this simulation algorithm with a discussion of its dynamical features is contained in Ref. [2]. Data relative to the largest lattices for $N = 21$ and $N = 41$ are taken from Ref. [8] where

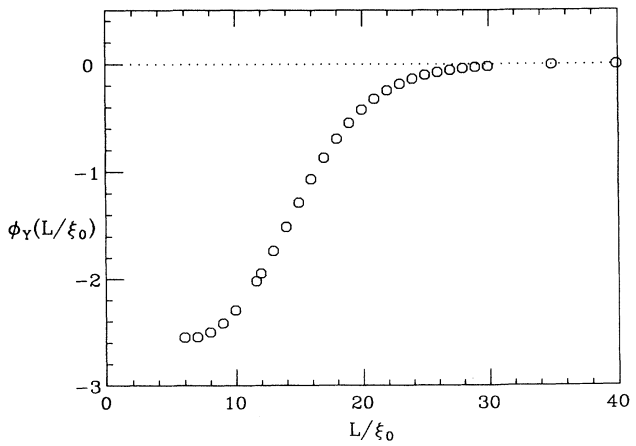

FIG. 11. $\phi_Y(L/\xi_0)$ for $\xi_0 = 16.04$.

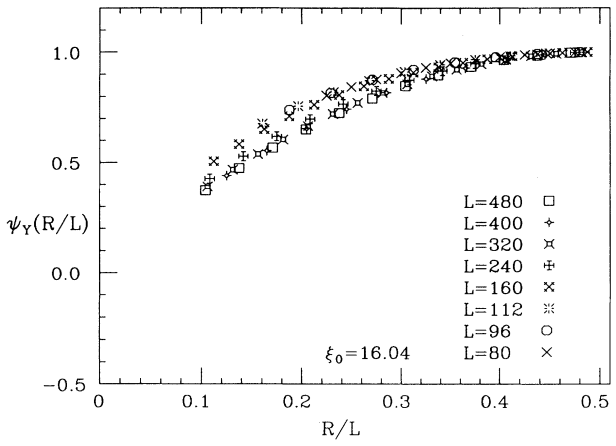

FIG. 12. $\psi_Y(R/L)$ for $\xi_0 = 16.04$ and for several values of L.

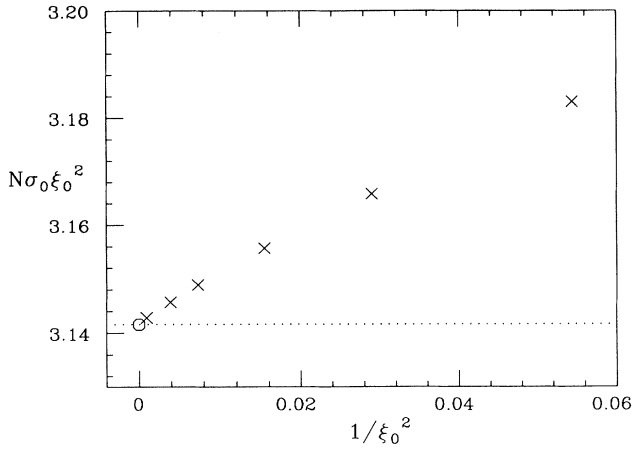

FIG. 13. The large-N string tension on the lattice at finite ξ_0. $N\sigma_0\xi_0^2$ is plotted versus $1/\xi_0^2$.

the simulated tempering algorithm [10] was employed.

By varying the lattice size at fixed β we managed to reconstruct the finite size functions $f^{(\chi)}$ and $f^{(\xi)}$. They were obtained by approximating infinite lattice quantities with the corresponding values measured on the largest lattice available for each β and N (of course after checking the stability of the results on large lattices). The results relative to $f^{(\chi)}$ and $f^{(\xi)}$ are plotted, respectively, in Figs. 14 and 15 for $N = 100$, in Figs. 16 and 17 for $N = 41$, in Figs. 18 and 19 for $N = 21$, in Figs. 20 and 21 for $N = 10$. In these figures the dashed lines show the large-N predictions (31), and the continuous lines represent the inclusion of the $1/N$ correction evaluated in Sec. III.

In the scaling region the finite size scaling functions must be universal, that is independent of β and of the lattice formulation, in that they should reproduce the continuum physics in a periodic box. Data for $N = 10, 21, 41$ coming from different β values show this universal behavior.

A summary of all the most significant results is presented in Figs. 22 and 23 where all different values of N are brought together, including data for $N = 2$ and $N = 4$, in order to see the general trends.

As anticipated in Sec. III, two physically distinct regions exist. In the small volume domain the $1/N$ expansion (as well as the perturbative expansion) is predictive for values of N as small as 10. The vanishing of $f_1^{(\chi)}$ in a neighborhood of $L/\xi \simeq 3$ reflects itself in the approximate universality of the corresponding finite size curves in the same region for all $N \geq 4$. The large volume behavior shows a peculiar disagreement with the $1/N$ expansion: convergence to the infinite volume prediction is much faster than expected even for rather large values of N and moreover, it follows a pattern that does not seem to be amenable to analytic $1/N$ effects.

Actually there is a plausible interpretation of this phenomenon, as we shall try to show. One must not forget that the physical spectrum of CP^{N-1} models is characterized by effects of confinement, that in turn leads to

TABLE I. Large-N string tension versus β.

β	ξ_0	$N\sigma_0\xi_0^2$
0.54	2.1474	3.2709
0.65	4.2859	3.1827
0.70	5.8678	3.1658
0.75	8.0337	3.1557
0.81	11.7123	3.1489
0.86	16.0350	3.1457
0.97	32.0067	3.14284
∞	∞	3.14159...

TABLE II. Summary of the simulation results for the CP^9 model.

β	L	E	ξ	χ_m
0.75	18	0.7157(3)	3.71(2)	19.39(11)
	21	0.7179(2)	3.61(2)	18.66(10)
	24	0.7196(2)	3.43(2)	17.62(8)
	27	0.7198(2)	3.34(2)	17.16(8)
	30	0.7202(1)	3.289(15)	16.94(5)
	42	0.7202(1)	3.27(3)	16.80(5)
	48	0.7202(1)	3.25(3)	16.77(4)
	54	0.7202(1)	3.31(3)	16.80(4)
	60	0.7203(1)	3.31(4)	16.79(4)
0.8	9	0.6473(5)	3.377(9)	17.25(4)
	12	0.6539(4)	4.070(13)	22.88(7)
	18	0.6606(3)	5.02(2)	30.88(12)
	24	0.6642(2)	5.19(3)	32.19(23)
	27	0.6650(2)	5.18(3)	32.14(21)
	30	0.6659(2)	5.07(4)	31.07(23)
	33	0.6668(2)	4.79(3)	29.29(17)
	36	0.6667(1)	4.70(4)	28.75(17)
	39	0.6669(1)	4.67(3)	28.56(13)
	48	0.66689(6)	4.60(2)	28.14(8)
	60	0.66699(4)	4.60(2)	28.08(5)
0.85	15	0.6145(3)	5.221(16)	34.20(10)
	36	0.6213(1)	7.21(5)	53.63(43)
	48	0.62196(9)	6.63(5)	48.73(32)
	60	0.62216(8)	6.48(5)	47.41(26)
	72	0.62214(8)	6.44(6)	47.18(22)

TABLE III. Summary of the simulation results for the CP^{20} model.

β	L	E	ξ	χ_m
0.65	6	0.7550(4)	2.041(3)	8.562(13)
	9	0.7767(4)	2.611(6)	11.96(3)
	12	0.7864(3)	2.989(8)	13.99(4)
	15	0.7914(2)	3.193(8)	14.84(4)
	18	0.7950(2)	3.186(17)	14.49(8)
	21	0.7976(2)	3.003(19)	13.43(8)
	24	0.7990(2)	2.835(17)	12.67(6)
	30	0.7992(1)	2.721(13)	12.26(4)
	36	0.7993(1)	2.696(13)	12.17(3)
	42	0.7995(1)	2.691(18)	12.14(3)
0.7	6	0.7004(6)	2.239(4)	9.767(17)
	9	0.7191(4)	2.957(7)	14.65(3)
	12	0.7267(3)	3.524(7)	18.58(4)
	30	0.7388(2)	4.19(6)	21.74(25)
	36	0.7389(2)	3.83(3)	19.9(1)
	48	0.7392(2)	3.716(25)	19.51(8)

TABLE IV. Summary of the simulation results for the CP^{40} model.

β	L	E	ξ	χ_m
0.57	6	0.8440(6)	1.764(3)	7.049(12)
	9	0.8672(3)	2.163(4)	8.876(19)
	12	0.8781(2)	2.358(4)	9.44(2)
	15	0.8830(2)	2.406(8)	9.30(3)
	18	0.8863(2)	2.292(7)	8.67(2)
	21	0.8888(2)	2.078(9)	7.97(2)
	24	0.8887(1)	2.032(8)	7.85(15)
	33	0.8889(1)	2.004(7)	7.755(9)
	42	0.8890(1)	2.011(10)	7.756(8)
0.6	6	0.8007(6)	1.897(4)	7.853(16)
	9	0.8235(5)	2.398(6)	10.51(3)
	12	0.8340(3)	2.701(6)	11.84(3)
	15	0.8385(2)	2.864(7)	12.25(3)
	18	0.8415(2)	2.902(10)	12.07(4)
	42	0.8454(1)	2.431(11)	10.105(15)

TABLE V. Summary of the simulation results for the CP^{99} model.

β	L	E	ξ	χ_m
0.54	6	0.8749(4)	1.670(2)	6.590(9)
	9	0.8988(2)	2.037(4)	8.11(2)
	12	0.9088(2)	2.221(5)	8.53(2)
	15	0.9135(2)	2.263(5)	8.344(16)
	18	0.9164(1)	2.210(6)	7.936(17)
	21	0.9177(1)	2.111(5)	7.541(12)
	24	0.9188(2)	2.011(7)	7.278(13)
	36	0.91899(7)	1.916(8)	7.078(7)
	42	0.91895(5)	1.916(8)	7.072(5)
	48	0.91893(7)	1.922(9)	7.069(6)

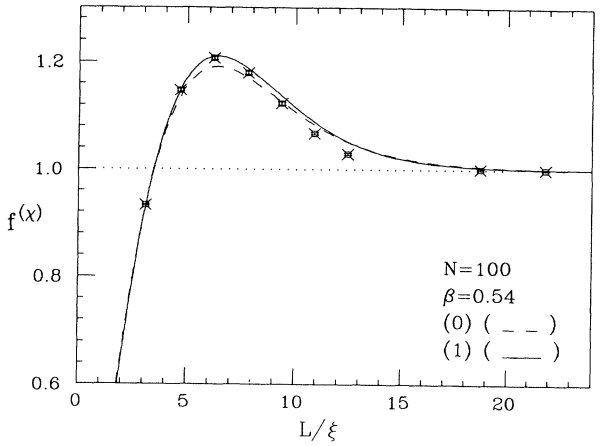

FIG. 14. Finite size scaling of the magnetic susceptibility for $N = 100$. The dashed and the continuous lines show, respectively, the leading and the next-to-leading order of the large-N expansion.

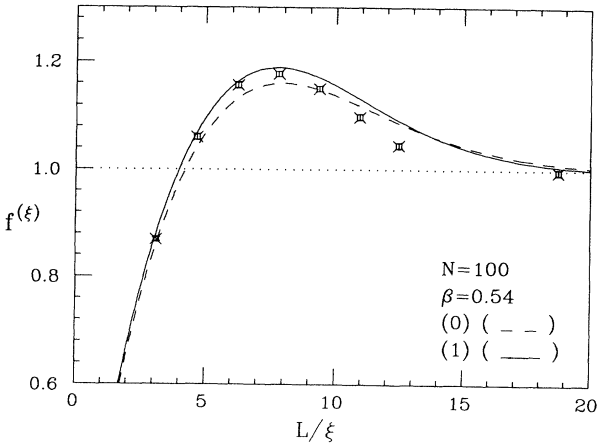

FIG. 15. Finite size scaling of the correlation length for $N = 100$. The dashed and the continuous lines show, respectively, the leading and the next-to-leading order of the large-N expansion.

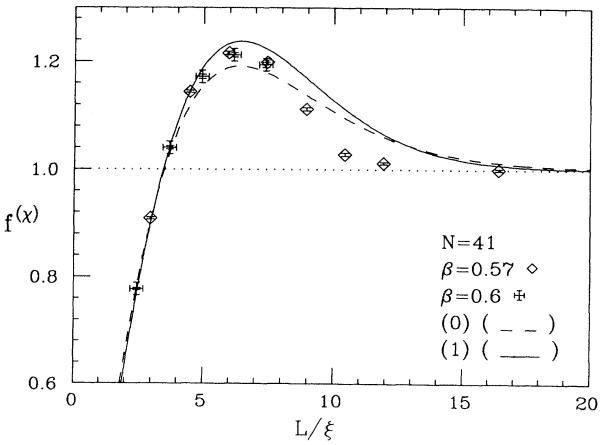

FIG. 16. Finite size scaling of the magnetic susceptibility for $N = 41$. The dashed and the continuous lines show, respectively, the leading and the next-to-leading order of the large-N expansion.

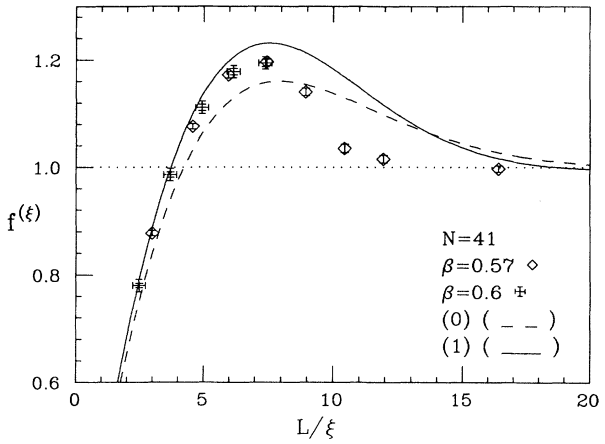

FIG. 17. Finite size scaling of the correlation length for $N = 41$. The dashed and the continuous lines show, respectively, the leading and the next-to-leading order of the large-N expansion.

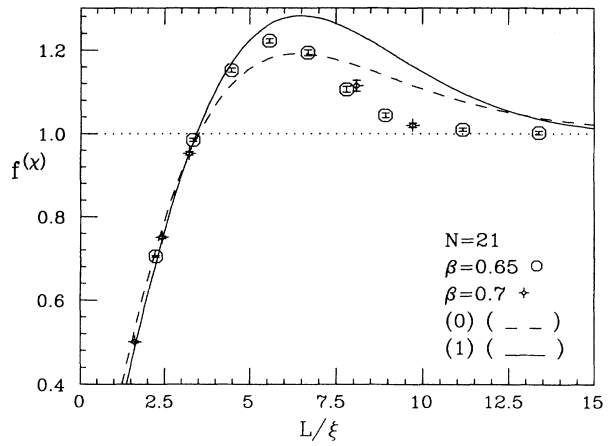

FIG. 18. Finite size scaling of the magnetic susceptibility for $N = 21$. The dashed and the continuous lines show, respectively, the leading and the next-to-leading order of the large-N expansion.

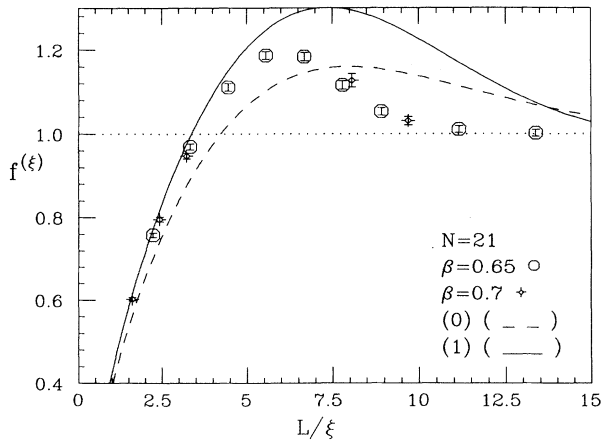

FIG. 19. Finite size scaling of the correlation length for $N = 21$. The dashed and the continuous lines show, respectively, the leading and the next-to-leading order of the large-N expansion.

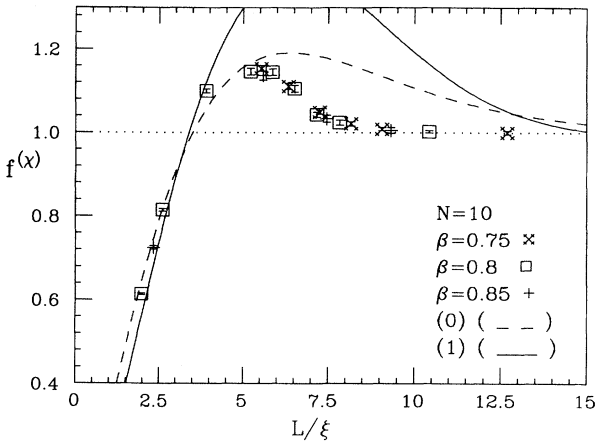

FIG. 20. Finite size scaling of the magnetic susceptibility for $N = 10$. The dashed and the continuous lines show, respectively, the leading and the next-to-leading order of the large-N expansion.

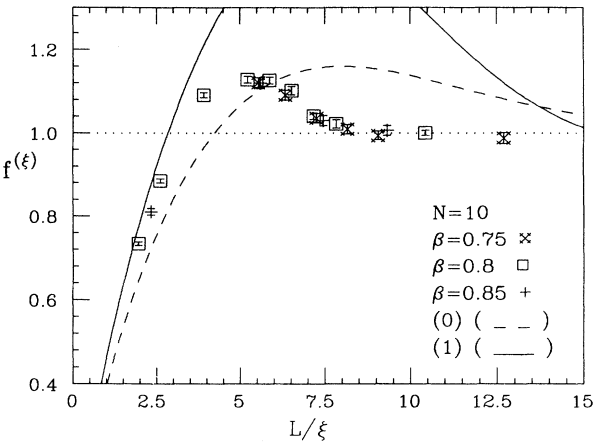

FIG. 21. Finite size scaling of the correlation length for $N = 10$. The dashed and the continuous lines show, respectively, the leading and the next-to-leading order of the large-N expansion.

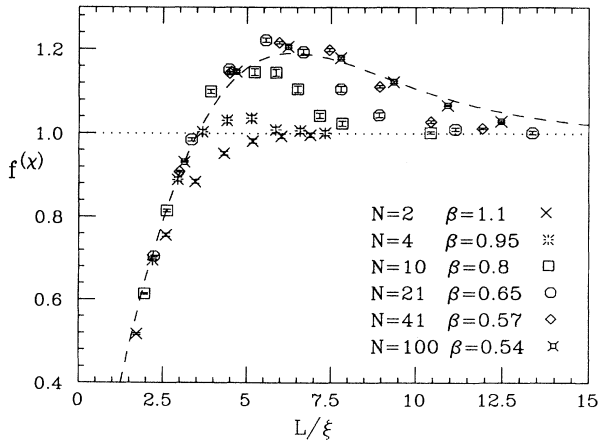

FIG. 22. Finite size scaling function of the magnetic susceptibility obtained by Monte Carlo simulations for several values of N. The dashed line shows the leading order of the large-N expansion.

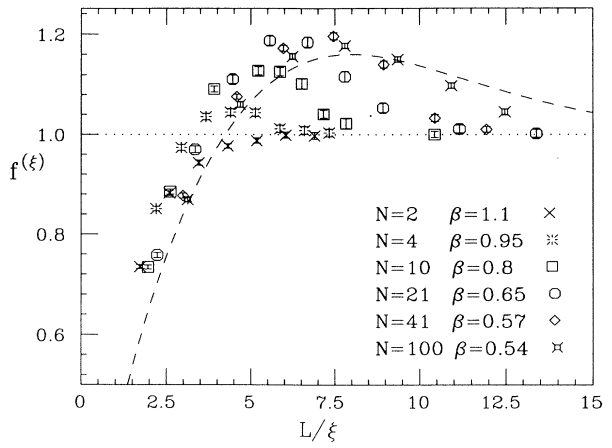

FIG. 23. Finite size scaling function of the correlation length obtained by Monte Carlo simulations for several values of N. The dashed line shows the leading order of the large-N expansion.

the appearance of two-particle bound states, dominating the large-distance behavior of the function G_P. These bound states have binding energies order $(6\pi/N)^{2/3}$ that are nonanalytic in $1/N$, and physical extension (effective radius) order $(N/6\pi)^{1/3}$. Therefore they will dominate the finite size effects on large lattices ($L \sim N^{1/3}\xi$), while in the intermediate region the finite size functions must interpolate between the analytic (small volume) and the nonanalytic behavior. We may therefore expect these functions, for intermediate values of N, to show a (roughly) universal behavior for intermediate and large values of the effective variable $L/(\xi N^{1/3})$. This effect is shown in Figs. 24 and 25, where this kind of universality is shown to apply to values $4 \leq N \leq 41$. There is necessarily a saturation effect, because otherwise the convergence to infinite volume results would be further delayed for larger values of N, in contrast with the $N \to \infty$ prediction. Indeed at $N = 100$ we see a significant departure from the $\xi N^{1/3}$ scaling and an improved agreement with the $1/N$ expansion even in the large volume regime.

At the opposite end of our analysis, when $N = 2$ we find that none of the previous considerations apply, but for the obvious agreement at small L/ξ due to the predictivity domain of standard perturbation theory (that commutes with the $1/N$ expansion). CP^1 is equivalent to the O(3) nonlinear σ model, and the finite size curves are actually showing the typical behavior of single-particle correlations in a finite volume (free particle in a box). We stress however that this different qualitative pattern seems to come out without any quantitative discontinuity in the dependence on N, that appears to be monotonic and smooth in the whole range of the variable.

The infinite lattice correlation lengths obtained from our Monte Carlo simulations can be compared with those predicted by the $1/N$ expansion. From Eqs. (30) and (38) we can get $\xi(\beta)$ up to $O(1/N)$. For $N = 100$ and $\beta = 0.54$ we find $\xi = 1.9106$, to be compared with the corresponding Monte Carlo result on the largest available lattice: $\xi = 1.922(9)$ (see Table V). In the continuum the $1/N$ expansion of ξ leads to [9]

$$\xi\Lambda_L = \frac{1}{8\sqrt{3}}\left[1 - \frac{6.7033}{N} + O\left(\frac{1}{N^2}\right)\right] , \qquad (65)$$

where Λ_L is the Λ parameter of the lattice action (9). Assuming asymptotic scaling, according to the two-loop formula,

$$g(\beta) = (2\pi\beta)^{-2/N} \exp(2\pi\beta) , \qquad (66)$$

we can find the correlation length as a function of β: $\xi(\beta) = (\xi\Lambda_L)g(\beta)$. For $N = 100$ and $\beta = 0.54$ this would give $\xi = 1.955$, consistent with $O(1/N\beta)$ deviations from asymptotic scaling.

The string tension is easily extracted by measuring the square Creutz ratios $\chi_C(R,R)$; indeed for $L, R \gg \xi$ we should have

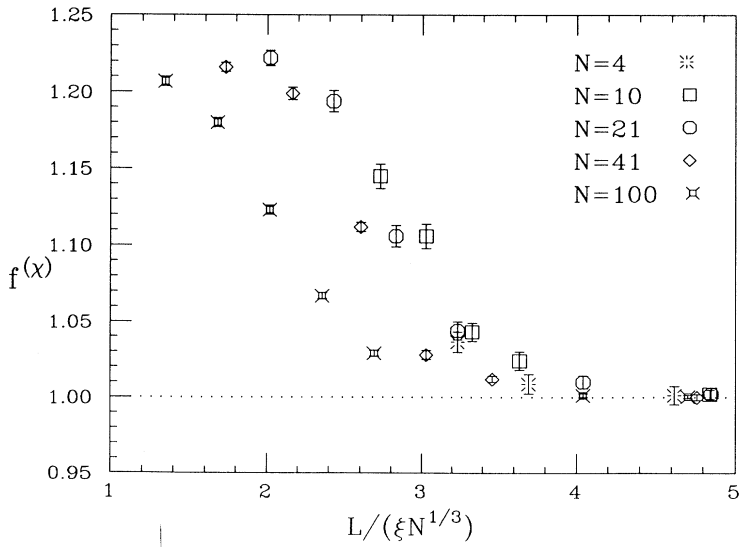

FIG. 24. Finite size scaling function of the magnetic susceptibility versus $L/(\xi N^{1/3})$.

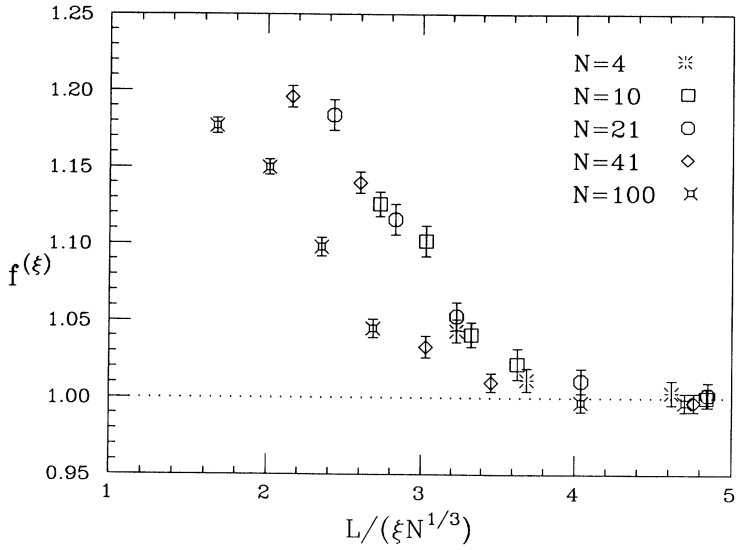

FIG. 25. Finite size scaling function of the correlation length versus $L/(\xi N^{1/3})$.

$$g^{(C)}(R) = \frac{\chi_C(R,R)}{\left[1-\left(\frac{2R-1}{L}\right)^2\right]}\xi^2 \to \sigma\xi^2 \quad . \tag{67}$$

As shown in Sec. III, in practice the factor $\left[1-\left(\frac{2R-1}{L}\right)^2\right]$ allows us to perform the measurement without requiring $L \gg R$. The string tension has been already measured for $N = 4$, $N = 10$ [7], $N = 21$, and $N = 41$ [8], showing for the last two values of N agreement with the large-N prediction $\sigma\xi^2 = \pi/N$. We have repeated the measurement for $N = 100$, at $\beta = 0.54$ on a $L = 48$ lattice, corresponding to $L/\xi \simeq 25$. In Fig. 26 $g^{(C)}$ is plotted versus the physical distance $r = R/\xi$; the continuous and the dashed lines show the large-N predictions obtained from Eq. (43) at the same bare coupling $\beta = 0.54$, respectively, for an infinite and an $L = 48$ lattice. The analysis done in Sec. IV and the small differences between the infinite and the $L = 48$ lattice predictions show that $L/\xi \simeq 25$ should be sufficient to determine the string tension through the measure of $g^{(C)}$. Monte Carlo data are consistent with the large-N results, which also predict the observed discrepancy of the measured string tension from the continuum value $\sigma\xi^2 = \pi/N$ due to scaling violations (see Table I and Fig. 13).

Finally we would like to make a few remarks on the study of the topological properties of CP^{N-1} models on the lattice. At large N a particularly severe form of critical slowing down, exponential with respect to correlation length, has been observed when measuring the topological susceptibility [2]. Moreover, this phenomenon becomes worse with increasing N, making the simulations effectively nonergodic, already at small ξ. In order to overcome this difficulty and to perform simulations sampling correctly the topological sectors at large N, in Ref. [8] the simulated tempering method of updating [10] was employed, and agreement with the large-N result $\chi_t\xi^2 = 1/(2\pi N)$ was found for $N = 21$ and $N = 41$.

At large N we expect that the dynamically generated

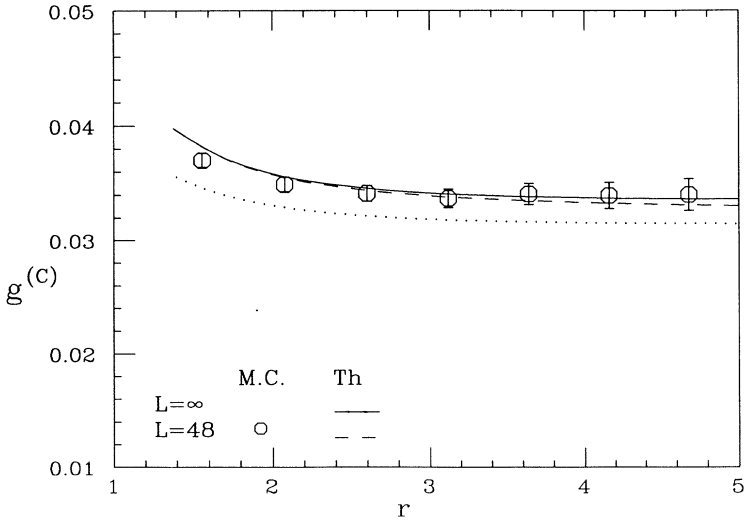

FIG. 26. Rescaled Creutz ratios versus $r = R/\xi$ for $N = 100$. Data were taken at $\beta = 0.54$ and on a $L = 48$ lattice. The continuous and the dashed lines show the large-N predictions obtained at $\beta = 0.54$, respectively, for an infinite and an $L = 48$ lattice. The dotted line is the $\beta \to \infty$ prediction, with asymptotic value π/N.

gauge field shows a phenomenon similar to that observed in the two-dimensional U(1) gauge model [11], that is a strong decoupling in the infinite-volume limit between the Gaussian modes around the large-N saddle point, responsible for confinement, and the modes determining the topological properties. A manifestation of this decoupling would be the possibility to obtain good estimates of observables not related to the topological properties even in simulations not sampling correctly the topological sectors [8]. Relying on this decoupling property we decided to use a local algorithm to perform our simulations at large N.

For $N = 100$ different topological sectors are separated by such a high free energy barrier that, starting from a flat configuration, even after a long thermalization procedure, we found zero geometrical charge for each configuration generated in our simulations. All our $N = 100$ results reported in Table V are effectively obtained by sampling configurations with $Q_g = 0$. We also found that the geometrical charge Q_g remained unchanged even when starting from a configuration having $Q_g \neq 0$. As expected, the measured values of χ_m, ξ, and $\chi_C(R, R)$ with $R \ll L$ become independent of Q_g for large enough lattices (and for reasonable values of Q_g). Anyway, since the large-N saddle point configuration has trivial topology, for all finite lattices the correct procedure to obtain reliable results is starting from a flat configuration and therefore effectively sampling configurations with $Q_g = 0$. The good agreement of the numerical results obtained in this way with the large-N predictions is a further support to the above-mentioned decoupling phenomenon.

VI. CONCLUSIONS

The analytical and numerical results we have presented lead to some considerations whose relevance might go beyond the domain of CP^{N-1} models.

(I) There is a perturbative domain for finite size effects, where it is possible to compute the finite size functions with satisfactory precision, both in the $1/N$ and in the standard weak coupling expansion. For asymptotically free theories, this domain coincides with the small volume regime. In the spirit of Lüscher and collaborators' investigations [4,12], one might conceive of supplementing the perturbative evaluations with numerical simulations at rather small volumes and matching numerical finite size effects (functions of L/ξ) with analytical results (functions of ΛL) in order to extract physical information (e.g., the quantity $\Lambda\xi$).

(II) In the presence of a confining potential, bound states have a physical radius that can be significantly bigger than the correlation length appearing in the long distance behavior. This new physical scale may dominate the finite size effects on volumes that are large with respect to the correlation length but comparable with the bound-state radius itself.

(III) Phenomena related to topological properties show peculiar finite lattice behaviors. Actually our calculations have shown that assuming to define a topological susceptibility by the standard (continuum or infinite lattice) procedure

$$\chi_t = \lim_{k \to 0} \widehat{k}^2 \Delta_{(\lambda)}(k) \quad , \tag{68}$$

the result would be zero on any finite lattice because the dynamically generated massless pole disappears on finite lattices, as expected on general theoretical grounds. As we have seen, this is also the reason why it is, strictly speaking, impossible to give a definition of the string tension on finite lattices. However one must not forget that the infinite-volume limit is reached smoothly and the convergence, for sufficiently large L, becomes exponentially fast (water boils also in your pot, and not only in the infinite-volume limit). Therefore it should always be possible, with an appropriate limiting procedure, to extract infinite-volume information from finite-volume simulations. We have seen that careful handling leads to the possibility of "measuring" the string tension on finite lattices within the desired precision. Similarly, we see no obstruction to interpreting the so-called "geometrical" definitions of topological charge (and derived quantities) as limits of sequences of local operators [2] that can be approximately evaluated on finite lattices, thus giving a precise meaning to apparently ill-defined quantities.

[1] M. Campostrini and P. Rossi, Phys. Lett. B **255**, 89 (1991).
[2] M. Campostrini, P. Rossi, and E. Vicari, Phys. Rev. D **46**, 2647 (1992).
[3] M. Campostrini and P. Rossi, Phys. Rev. D **45**, 618 (1992); **46**, 2741(E) (1992).
[4] M. Lüscher, Phys. Lett. **118B**, 391 (1982).
[5] P. Hasenfratz, Phys. Lett. **141B**, 385 (1984).
[6] H. Flyvbjerg, J. Phys. A **22**, 3393 (1989).
[7] M. Campostrini, P. Rossi, and E. Vicari, Phys. Rev. D **46**, 4643 (1992).
[8] E. Vicari, Phys. Lett. B **309**, 139 (1993).
[9] M. Campostrini and P. Rossi (unpublished).
[10] E. Marinari and G. Parisi, Europhys. Lett. **19**, 451 (1992).
[11] M.L. Laursen, J. Smit, and J.C. Vink, Phys. Lett. B **262**, 467 (1991).
[12] M. Lüscher, P. Weisz, and U. Wolff, Nucl. Phys. **B359**, 221 (1991).